Upon further cooling an anisotropic distortion appears at T_N accompanied by a change of the lattice symmetry. In the following, we will proceed to the analysis of the structural transition observed at T_N.

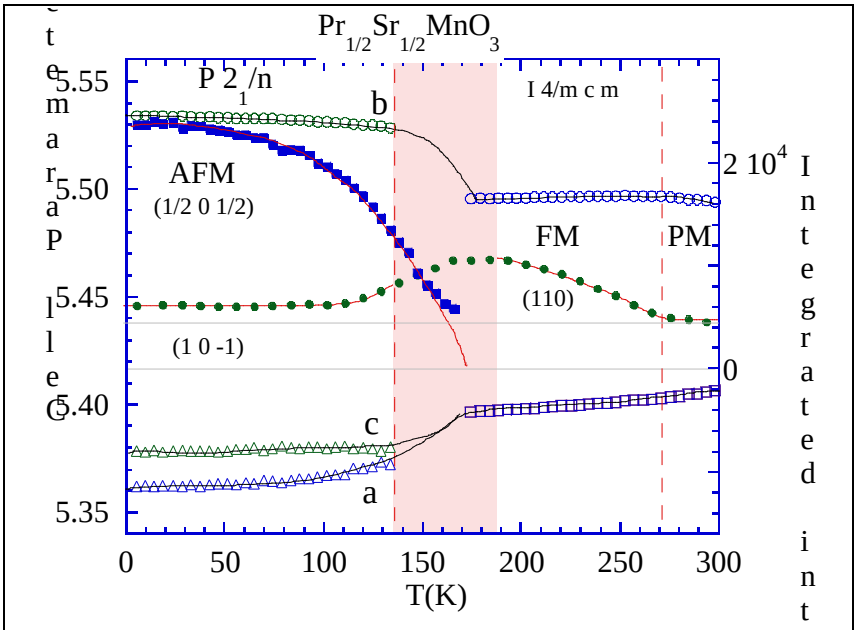

Fig. 6-6 *Thermal evolution of the cell parameters of $Pr_{1/2}Sr_{1/2}MnO_3$ as extracted from D1B powder diffraction patterns. The integrated intensity of the A-type AFM (1/2 0 1/2) peak and of the (110) peak of I4/mcm simetry which has contribution of the FM order.*

The high temperature tetragonal structure remains stable down to about 140K. Below this temperature, several remarkable features in the neutron diffraction pattern are:

a) Presence of new magnetic peaks which can be associated to an A-type AF magnetic order.

b) Structural peaks of the metallic FM I4/mcm phase split into separated reflections below T_N

c) Crystal symmetry change.

In Fig. 6-7 is shown the evolution of the integrated intensities of the $(10\text{-}1)_M$ and $(101)_M$ reflections illustrating the monoclinic splitting of the $(110)_T$ tetragonal reflection. The $(110)_T$ reflection is also the most intense magnetic reflection in ferromagnetic manganites with the moments along the *c* axis, so the increase of intensity reflects also the FM contribution.

Below T_N, the D2B NPD pattern was satisfactorily fitted using the $P2_1/n$ (a= 5.3720(4)Å, b=7.8282(4)Å, c=5.3740(5)Å, β=91.303(4)°) monoclinic space group. The fits improved when an additional phase was included which corresponds to a non-transformed residual phase (11% in volume) presenting the high temperature structure. The results of the best fits are shown in Tab. 6-III and the fitted NPD pattern is shown in Fig. 6-10. The coexistence at low temperatures of two states

with similar energy is a common feature in manganites [151]. Nevertheless, other authors have observed single phase at low temperature [152].

The magnetic structure was identified as an A-type magnetic structure, which is associated to the apparition of intensity in the (1/2 0 1/2) reflection, with FM moments in the *b* direction and FM planes being the (1 0 1) planes in the P1 $2_1/n$ 1 setting. This result contrasts with the one obtained in $LaMnO_3$ where the FM planes were the (0 1 0) planes (Pnma symmetry) [19]. The ordered AFM moment found in the $Pr_{1/2}Sr_{/2}MnO_3$ monoclinic phase was about 3.5μ_B/Mn ion which agrees with the theoretical spin only value expected for _ of Mn^{+3} and _ of Mn^{+4}. The residual tetragonal phase presented a FM moment of about 3.3(1)μ_B/Mn .

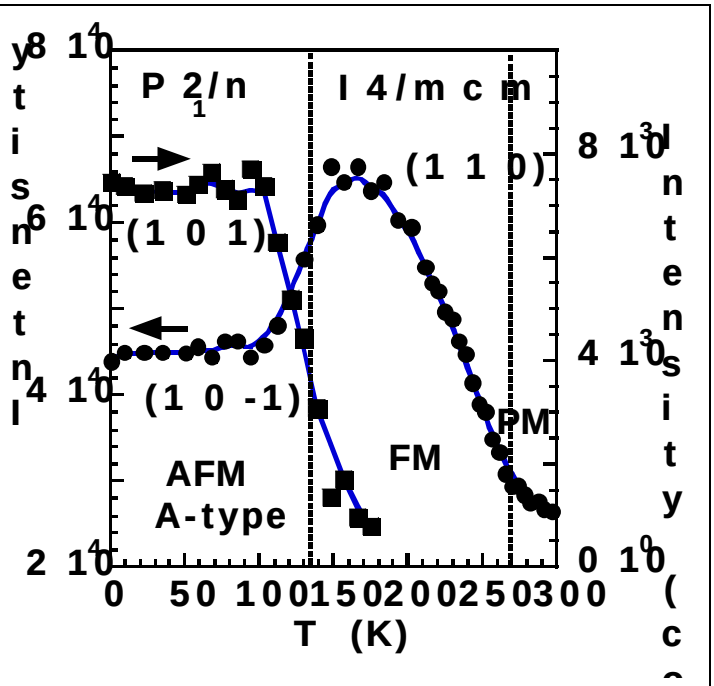

Fig. 6-7 *Evolution of the monoclinic splitting of the (110) tetragonal reflection and magnetic transitions*

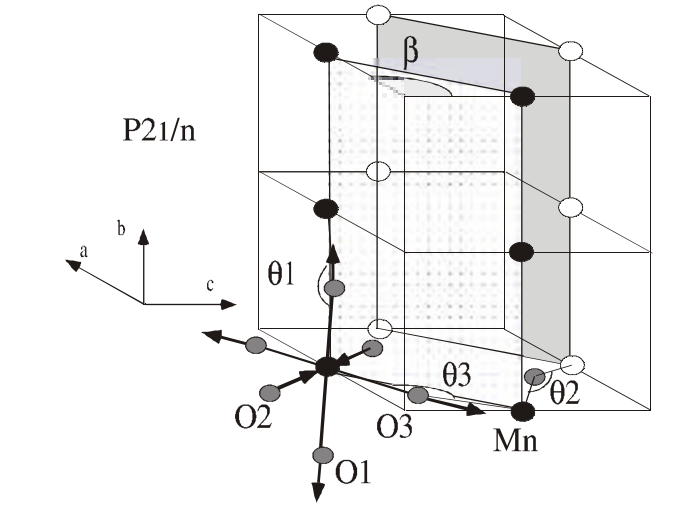

Fig. 6-8 *Schematic representation of the $P2_1/n$ a layered structure of $Pr_{1/2}Sr_{1/2}MnO_3$ showing the deformations responsible for the I4/mcm (FM) to $P2_{1/n}$ (AFM) transition.*

In $P2_1/n$ symmetry, there are two crystallographically different Mn positions (Mn1 and Mn2) and three nonequivalent oxygen atoms (O1, O2, O3), all in general positions (Fig. 6-8). A charge ordered state in the A-type AFM state is permitted in this crystal symmetry. If charges were ordered we would expect the coexistence of expanded (Mn^{+3}) and contracted (Mn^{+4}) octahedra, which could be nicely described by the $P2_1/n$ space group. An example of charge disproportion displaying such order ($P2_1/n$) can be found in the $YNiO_3$ compound [153].

In Tab. 6-I are shown selected distances and angles of this compound at several temperatures. From the refinements of the 1.5K D2B NPD pattern we concluded that within the error, the Mn-O distances in the Mn1 and Mn2 octahedra were very similar meaning that not such charge order exist in $Pr_{1/2}Sr_{1/2}MnO_3$. Final refinements were thus made with constrained Mn-O distances, supposing equally deformed octahedra. The agreement factors were satisfactory taking into account that we were dealing with 2 nuclear and 2 magnetic phases (R_N= 7.2%).

In conclusion, the fact that the diffraction patterns agreed with equally deformed octahedra, permits to assure that no static order of the charges giving rise to Mn^{+3}/ Mn^{+4} order exist in this compound. The charges seem to be homogeneously distributed in $Pr_{1/2}Sr_{1/2}MnO_3$. Therefore, at variance with the Pnma-$P2_1/n$, metal-insulator transition in $YNiO_3$ perovskite, the origin of the monoclinic symmetry is not a charge ordered state. This result contradicts with the assumptions in [154] and [147], which interpreted ρ(H,T) and M(H,T) measurements as a proof of CO in $Pr_{1/2}Sr_{1/2}MnO_3$.

Tab. 6-I *Selected interatomic distances and angles of* $Pr_{0.50}Sr_{0.50}MnO_3$ *at* $1.5K$ *, 200 K and RT.*

	1.5K	200 K	RT
	P $2_1/n$	*I* 4/*mcm*	*I* 4/*mcm*
$d_{Mn-O(1)}(Å)$	1.9577(8)	1.9398(6)	1.9378(6)
$d_{Mn-O(2)}(Å)$	1.897(2)	1.923(2)	1.924(2)
$d_{Mn-O(3)}(Å)$	1.936(2)	"	"
$d_{equat}(Å)$	1.917(2)	1.923(2)	1.924(2)
$\langle d_{Mn-O}\rangle(Å)$	1.930(2)	1.928(2)	1.928(2)
θ_1=Mn-O1-Mn (deg)	176.89(8)	180	180
θ_2=Mn-O2-Mn (deg)	163.6(5)	164.4(5)	165.1(5)
θ_3=Mn-O3-Mn (deg)	165.9(5)	"	"
$\Delta d \times 10^4 = (1/6)\sum_{n=1,6}\left[(d_n - \langle d\rangle)/\langle d\rangle\right]^2 10^4$	1.67	0.17	0.11
$\varepsilon_d = \left\|\frac{d_{equat}}{d_{apic}} - 1\right\| \times 10^4$	210	86	72

The fact that there exists no difference in the Mn1 and Mn2 octahedra allows the possibility of using a space group in which no such difference between the Mn positions exists. In this sense, [155] reported the description of $Pr_{1/2}Sr_{1/2}MnO_3$ based on electron diffraction techniques (ED). These authors deduced from ED that the low temperature symmetry was an F type and thus found that the space group symmetry was Fmmm type and the cell was $2a_p \times 2a_p \times 2a_p$, instead of our smaller cell $\sqrt{2}a_p \times 2a_p \times \sqrt{2}a_p$. This space group gave satisfactory results in their NPD Rietveld refinements. Nevertheless, this symmetry does not allow the existence of two different Mn sites (CO is precluded) and is impossible to distinguish it from the $P2_1/n$ space group in the present case when using high-resolution D2B NPD data. In Fig. 6-10 and Fig. 6-9 are compared the refined NPD patterns using the $P2_1/n$ and Fmmm space groups in our sample.

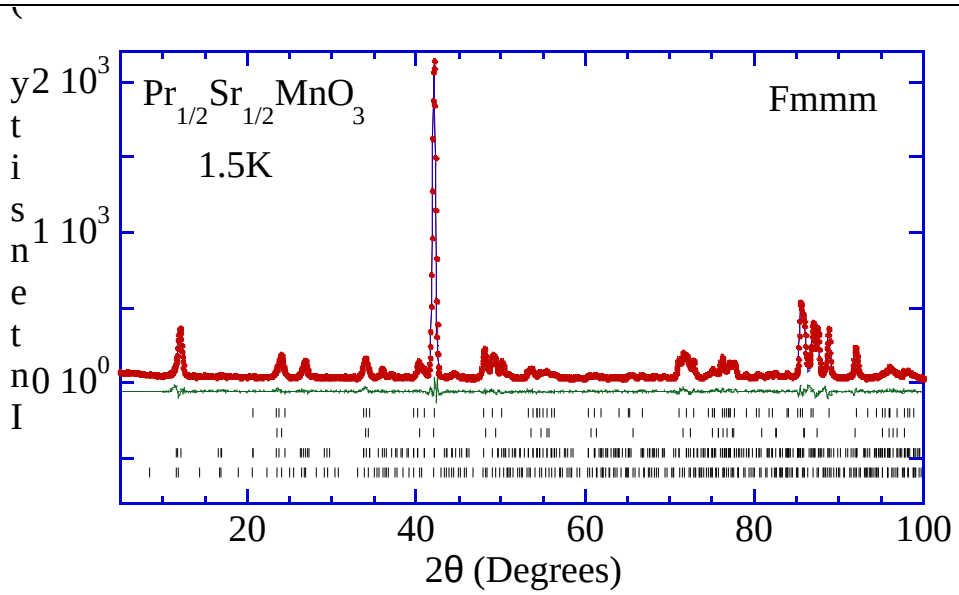

Fig. 6-9 *Observed (circles) and calculated (line) neutron-diffraction pattern of $Pr_{1/2}Sr_{1/2}MnO_3$ at 1.5 using the Fmmm space group suggested by[155].*

The results of the Rietveld refinements using these two space groups show similar reliability factors. Hence, from high resolution D2B NPD data we cannot distinguish which is the correct space group and unit cell. In Tab. 6-IV are shown the atomic positions obtained from the Rietveld refinements using the Fmmm space group, considering a bigger cell, compared with the ones of the $P2_1/n$. In the Fmmm space group, there exist only one Mn in a special position and the oxygen atoms are in y=0. In Tab. 6-II is shown selected interatomic distances and angles using both space groups.

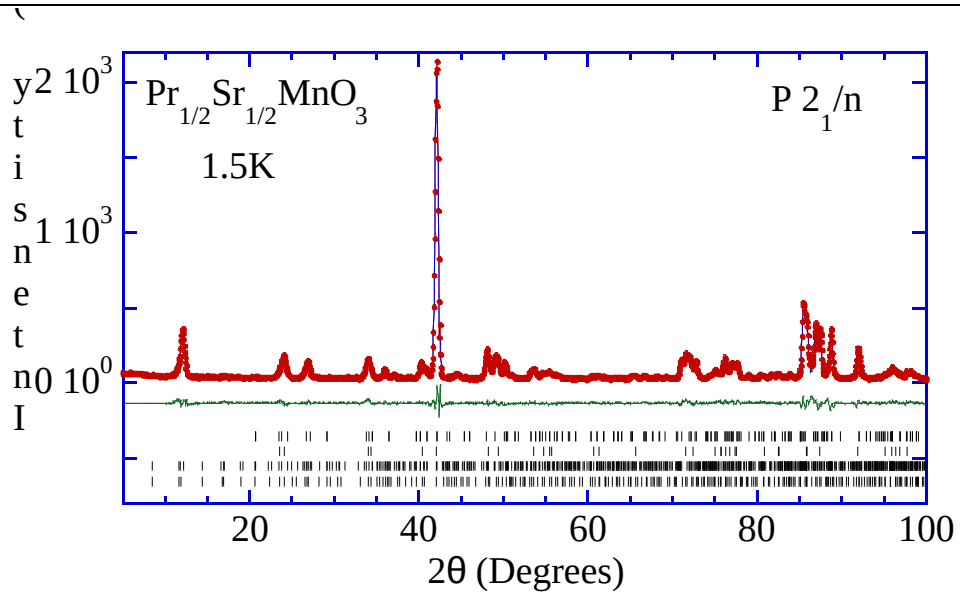

Fig. 6-10 *Observed (circles) and calculated (line) neutron-diffraction pattern of $Pr_{1/2}Sr_{1/2}MnO_3$ at 1.5 using $P2_1/n$ space group*

The relationship between the cells obtained in the two descriptions are sketched in Fig. 6-11. The cell parameters equivalence between the monoclinic $a' \approx \sqrt{2}a_p$, $b' \approx 2a_p$, $c' \approx \sqrt{2}a_p$ (and $\beta \neq 0$) cell and the orthorhombic $a \approx 2a_p$, $b \approx 2a_p$, $c \approx 2a_p$ are the ones that follow:

$$a' = c' = \sqrt{\left(\frac{a}{2}\right)^2 + \left(\frac{c}{2}\right)^2}$$
$$b' = b \qquad \textbf{Eq. 6-1}$$
$$\beta = 2 \times \arctan\left(\frac{c}{a}\right)$$

From the cell parameters obtained with the Fmmm description, we have calculated the cell parameters when transformed to the $P2_1/n$ description and we obtained: $a' \approx c' \approx 5.373$Å, $b' \approx 7.8282$Å and $\beta \approx 91.31°$. These values coincide, within the error, to the values obtained with the monoclinic description.

Mn atoms are in the same special position in both space groups and thus both descriptions should give rise to the same distance between FM planes. The position of the Pr and Sr atoms, after a change of the reference system, are very similar in both space groups.

The unique difference that can be appreciated between the descriptions using the two space groups and cells concerns the position of one oxygen atom. In Fig. 6-11 (b) are shown the MnO_2 planes with the oxygen positions from the refinement of the NPD of our sample. The main difference in the atomic position of the basal oxygens is that while in $P2_1/n$ symmetry they are in (x,y,z) general

position, in the Fmmm space group symmetry the oxygens lay in the y=0 plane. Within the error, the position of the oxygens obtained with the $P2_1/n$ space group (y(O2)=0.001(4) and y(O3)=-0.002(4)) is compatible with the requirement of the Fmmm space group.

Tab. 6-II: *Selected interatomic distances and angles of* $Pr_{0.50}Sr_{0.50}MnO_3$ *at* $1.5K$ *extracted from the fit with the P2₁/n and Fmmm space groups*

	P $2_1/n$	*Fmmm*
$d_{Mn-O(1)}(\text{Å})$	1.957(1)	1.957(1)
$d_{Mn-O(2)}(\text{Å})$	1.897(2)	1.898(1)
$d_{Mn-O(3)}(\text{Å})$	1.936(2)	1.936(1)
$d_{equat}(\text{Å})$	1.917(2)	1.917(3)
$\langle d_{Mn-O}\rangle(\text{Å})$	1.930(1)	1.930(1)
θ_1=Mn-O1-Mn	176.9(1)	180
θ_2=Mn-O2-Mn	163.6(5)	163.2(1)
θ_3=Mn-O3-Mn	165.9(5)	165.58(2
$\Delta_d \times 10^4$	1.67	1.60
$\left\|\frac{d_{equat}}{d_{apic}}-1\right\|\times 10^4$	210	203

Few changes are observed in distances and angles with respect to the values obtained with the $P2_1/n$ space group. The Mn-O distances obtained using the different space groups are the same. On the other hand, the smaller angle is in both cases the angle connecting the FM planes.

The main difference when using the Fmmm description is the Mn-O1-Mn apical angle. While in the case of the P21/n symmetry, the angle is free to vary and converged to a value of 177°, in the case of the Fmmm symmetry this angle is fixed to 180 °. Such difference is unable to modify the conducting character because the critical Mn-O-Mn angle for conducting character is about 163° as extracted from [145].

On the other hand, the θ_3 and θ_2 angles are very similar in both space group descriptions ($\theta_3 \approx 165°$and $\theta_2 \approx 163°$). The θ_3 angle is the angle controlling the exchange interaction between FM planes while θ_2 is the angle between the FM planes.

In conclusion, even if the space group determined by [155] as extracted from electron microscopy should be considered, from NPD data is not possible to distinguish between the small ($P2_1/n$) and the large (Fmmm) cell. Both descriptions give rise to the same contraction of the distances between FM planes ((1 01) in the $P2_1/n$ and (100) in the Fmmm space group). In what follows we have used the $P2_1/n$ description.

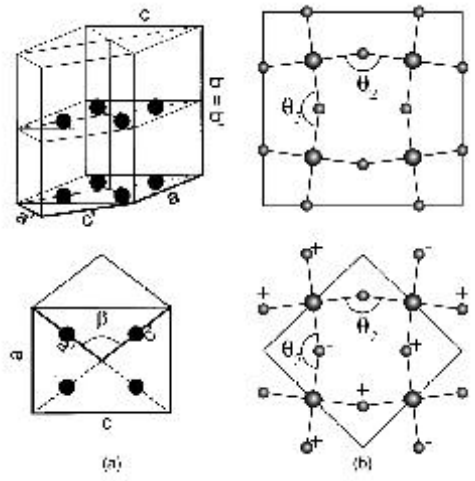

Fig. 6-11 *Comparison of the lattice corresponding the $P2_1/n$ an with a Fmmm.*

6.3 Interpretation: Orbital Ordering

In order to understand the physical origin of the I4/mcm- $P2_1/n$ transformation we have analysed the obtained Mn-O distances and Mn-O-Mn angles shown in Tab. 6-I. The main remarks from the inspection of the calculated distances are, firstly, that the mean Mn-O distances ($<d_{Mn-O}>$) in the tetragonal and monoclinic phase do not meaningfully change at T_N. Hence, no remarkable reduction of the oxygen octahedra volume is observed when crossing the structural transition. Secondly, the MnO_6 octahedra distortion (ε_d) is six times larger below T_N than above T_N. This distortion is smaller than the distortion found in $LaMnO_3$ ($\Delta_d=3.3\ 10^{-3}$ [156, 157]) but is larger than the distortion found in $La_{1/2}Ca_{1/2}MnO_3$ ($\Delta_d=0.9\ 10^{-4}$). In addition, the distance between FM planes (Mn-0_2) is reduced by 0.06 Å (1.6%) in the low temperature phase while the Mn-Mn distances in the FM planes have increased by 0.03 and 0.04 Å (0.7, 0.9%). Hence, it indicates that the structural reorganisation at T_N is very anisotropic.

The stretching distortion generated at T_N is sketched in Fig. 6-8. The tetragonal basal plane of the MnO_6 containing six identical bonds is deformed to give different bond lengths:

a) Mn-O1 and Mn-O3 bonds in the FM plane

b) Mn-O2 bond perpendicular to the FM planes

The Mn-O1 and Mn-O3 bonds are expanded at T_N while Mn-O2 is contracted with respect to RT values. There exists a pronounced contraction of the bond perpendicular to the ferromagnetic

planes ($\Delta_{Mn\text{-}O2}^{M\text{-}T}$=-0.027(2) Å) while the two bonds constituting the FM planes (Mn-O1 and Mn-O3) are expanded across the transition by 0.020(1) and 0.012(2) Å.

When considering the Mn-O-Mn angles, we observe that the angle within the FM planes (Mn-O_3-Mn) opens about 1° with respect to its value at 200K while the angle connecting the FM planes (Mn-O_2-Mn) is closed upon cooling by about 1°. In the DE scenario, the Mn-O-Mn bond angle controls the electron bandwidth and when the angle closes, the bandwidth is reduced. In Fig. 6-12 the distortion induced below T_N is schematically sketched. The combination of the evolution of the Mn-O-Mn angles combined with the evolution of the Mn-O distances induces the opening of the β angle and thus originates the symmetry change.

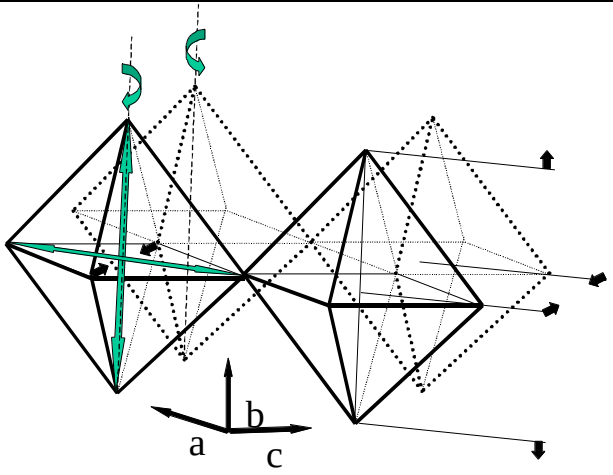

Fig. 6-12 *Schematic image of the distortion of the oxygen octahedra below T_N.*

The structural deformation is explained if we consider the thermal evolution of the selected distance and angles mentioned above between RT and 200K. The tendency upon cooling is to close Mn-O-Mn the angle between the FM planes and one of the Mn-O-Mn bond angles in the FM planes. This evolution would give rise to the existence of 1D FM and metallic chains when the narrowing of the angle between Mn in the FM planes attained a critical value. However, such state would lead to electronic instabilities and hence, the structural distortion would be energetically more favourable allowing the possibility to have metallic conduction and FM interaction within planes that couple AFM.

The parent compound $LaMnO_3$ with only Mn^{+3}, also displays an A-type AFM ordering. In this case, the changes in the Mn-O distances at the orbital ordering transition (T_{JT}=750K) are smaller for the Mn-O apical distance than for the Mn-O distances perpendicular to the FM planes [157]. In the case of $Pr_{1/2}Sr_{1/2}MnO_3$, the changes in the Mn-O2 bond length are larger than the changes in the other bonds thus indicating that the orbital ordering is different. In the case of $LaMnO_3$ there exist only Mn^{+3} which is Jahn-Teller distorted and the magnetic order is governed by superexchange interaction while in the case of $Pr_{1/2}Sr_{1/2}MnO_3$ the manganese ions can have two valence and the FM interaction is governed by the DE interaction which allows the FM planes to be metallic.

Recent theoretical calculations [158] suggest that in the heavily doped region (0.45<x<0.75) a second orbital structure is compatible with the stabilisation of the spin A type phase. They consider the possibility of partial hybridisation between the occupied and unoccupied bands ($(\alpha(x^2\text{-}y^2)\text{-}\beta(3z^2\text{-}r^2))$ with $\alpha>>\beta$). In the case α=1 it would be expected a completely absence of canting. Experimentally we

found the whole moment ($3.5\mu_B$/Mn ion) pointing in the *b* axis so we could explain the absence of FM coupling between the FM planes if we consider that the electrons are strictly localised in x^2-y^2 orbitals and no x^2-y^2 and $3z^2$-r^2 hybridisation (β=0).

Because of the occupation of the x^2-y^2 orbitals within the FM conducting planes, we would expect a reduction of the distance between the FM planes as observed experimentally. On the other hand the two identical angles in the tetragonal symmetry $\theta(2)$ and $\theta(3)$ are closed and opened respectively about 1° which disables the electronic transfer between the neighbouring FM planes.

6.4 Conclusions

From the above observations, it can be concluded that the metallic A-type antiferromagnetic structure appearing in $Pr_{1/2}Sr_{1/2}MnO_3$ appears due to electronic redistribution which causes the contraction of the Mn-O2 and expansion of Mn-O3 bonds and is compatible with the occupation of the x^2-y^2 orbitals in the FM planes, where 2D conduction probably exists.

At the FM/M-AFM/I transition there exists an electronic migration towards the FM planes due to the fact that the electron conduction between the planes is unfavoured because of the narrowing of the Mn-O-Mn angle perpendicular to the FM planes. Hence, in the present case, the structural transition is driven by the stabilisation of a particular orbital ordering in which the occupied orbitals are the x^2-y^2 type, within the FM planes. In other words, the driving force of the structural transition is the stabilisation of the x^2-y^2 orbital polarisation.

Tab. 6-III: *Refined structural parameters and reliability factors for* $Pr_{0.50}Sr_{0.50}MnO_3$

		1.5 *K*	200 K	RT
Parameter		*P* $2_1/n$	*I* 4/*mcm*	*I* 4/*mcm*
a (Å)		5.3720(4)	5.390(1)	5.398(1)
b (Å)		7.8282(4)	5.390(1)	5.398(1)
c (Å)		5.3740(5)	7.759(2)	7.756(2)
β (deg)		91.303(4)	90	90
Pr/Sr	*x*	0.500(4)	0	0
	y	0.7505(5)	1/2	1/2
	z	0.494(6)	1/4	1/4
B ($Å^2$)		0.15(7)	0.60(7)	0.66(7)
Mn1	*x*	0	0	0
	y	0	0	0
	z	1/2	0	0
B ($Å^2$)		0.11(8)	0.54(7)	0.85(7)
Mn2	x	1/2		
	y	0		
	z	0		
B ($Å^2$)		0.04(7)		
O1	*x*	-0.010(5)	0	0
	y	3/4	0	0
	z	0.501(4)	1/4	1/4
B ($Å^2$)		0.36(9)	1.0(1)	1.4(1)
O2	*x*	0.2852(4)	0.2173(5)	0.2173(5)
	y	0.001(4)	0.7173(5)	0.7173(5)
	z	0.7148(4)	0	0
B ($Å^2$)		0.60(7)	1.1(1)	1.4(1)
O3	*x*	0.7185(5)		
	y	0.502(4)		
	z	0.7185(5)		
B ($Å^2$)		0.62(7)		
Ordered Moment		AFM m_b=3.5(1)μ_B	FM m_C=3.3(1) μ_B	
R_N(%)		7.2	3.5	3.1
R_{Mag}(%)		7.0	5.2	

Tab. 6-IV: Refined structural parameters and reliability factors for $Pr_{0.50}Sr_{0.50}MnO_3$ using $P2_1/n$ and Fmmm space groups

		1.5 *K*	1.5K
Parameter		*P* $2_1/n$	*Fmmm*
	a (Å)	5.3720(4)	7.5107(2)
	b (Å)	7.8282(4)	7.8282(3)
	c (Å)	5.3740(5)	7.6843(3)
	β (deg)	91.303(4)	90
Pr/Sr	*x*	0.500(4)	0
	y	0.7505(5)	0.2506(5)
	z	0.494(6)	0
	B (Å^2)	0.15(7)	0.16(5)
Mn1	x	0	–
	y	0	0
	z	1/2	–
	B (Å^2)	0.11(8)	-0.15(7)
Mn2	x	1/2	
	y	0	
	z	0	
	B (Å^2)	0.04(7)	
O1	*x*	-0.010(5)	–
	y	3/4	–
	z	0.501(4)	–
	B (Å^2)	0.36(9)	0.48(6)
O2	*x*	0.2852(4)	0
	y	0.001(4)	0
	z	0.7148(4)	0.2861(4)
	B (Å^2)	0.60(7)	0.61(6)
O3	*x*	0.7185(5)	0.2176(5)
	y	0.502(4)	0
	z	0.7185(5)	0
	B (Å^2)	0.62(7)	0.61(6)
	Vol (Å^3)	451.78/2	451.78
	R_N(%)	7.2	6.9